

Resonant spatio-temporal forcing of oscillatory media

C. UTZNY¹, W. ZIMMERMANN^{1,2} and M. BÄR¹

¹ *Max-Planck-Institut für Physik komplexer Systeme
Nöthnitzer Str. 38, D-01187 Dresden, Germany*

² *Theoretische Physik, Universität des Saarlandes
D-66041 Saarbrücken, Germany*

(received 19 January 2001; accepted in final form 10 October 2001)

PACS. 82.40.Ck – Pattern formation in reactions with diffusion, flow and heat transfer.

PACS. 47.54.+r – Pattern selection; pattern formation.

Abstract. – An extension of the complex Ginzburg-Landau equation describing resonant spatio-temporal forcing of oscillatory media is investigated. Periodic forcing in space and time leads to spatial structures with two different symmetries: harmonic patterns with the same and subharmonic patterns with twice the wavelength of the external forcing. A linear stability analysis of the homogeneous state carried out analytically leads to subharmonic patterns for intermediate forcing strength, while harmonic modes prevail for very weak and strong forcing amplitudes. Numerical simulations confirm the analytical predictions for weak forcing and show coexistence between the two types of patterns beyond threshold. In addition, traveling localized patterns such as phase flips in subharmonic patterns and traveling patches of subharmonic patterns in a harmonic background have been discovered. In the parameter range of Benjamin-Feir turbulence, stable subharmonic patterns occur upon forcing, which undergo a transition scenario back to irregular dynamics for increasing values of the control parameter.

Introduction. – Resonant spatio-temporal forcing of pattern-forming systems combines two well-known strategies for the design and “control” of spatio-temporal dynamics: homogeneous resonant temporal forcing and spatial heterogeneities in the driving.

Pattern formation in the presence of spatially periodic modulation or randomly distributed heterogeneities has been investigated recently in hydrodynamical [1–3] and chemical [4–6] systems. Homogeneous, temporal forcing of oscillatory systems has been realized by variation of the external control parameter with n times the natural frequency (*e.g.*, $n = 1, 2, 3, 4$) [7]. Rich scenarios including phase-locked states and moving interfaces have been described for these resonantly forced systems theoretically [8–10] and experimentally for the light-sensitive ruthenium-catalyzed Belousov-Zhabotinsky reaction [11, 12]. Both control strategies are present in stochastic spatio-temporal forcing with random spatial heterogeneities and temporal forcing amplitudes, which has been studied in experiment [13] and theory [14, 15].

Here we combine forcing periodic in time *and* space applied to a complex Ginzburg-Landau equation and predict subharmonic patterns as a possible response. The model is a generalization of the equation used for 1 : 2 resonant forcing [8], where the homogeneous temporal forcing is replaced by a forcing with a spatially periodic modulated amplitude. In doing so, we enforce a typical length scale on the system and put a severe constraint by breaking the translational invariance of space and time. These broken symmetries are reflected by the

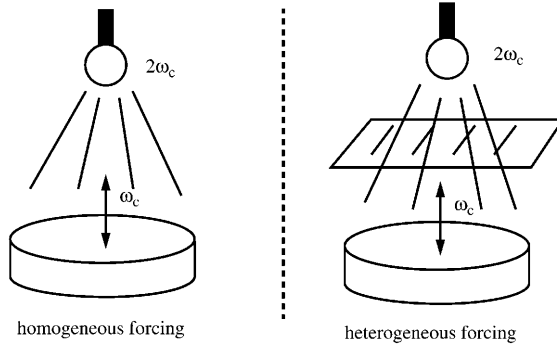


Fig. 1 – Sketch of a temporal forcing experiment with frequency ω_c (left) which may also be spatially modulated by a periodic filter (right).

shape of the critical modes destabilizing the homogeneous oscillation and thus by the spatial profiles of the resulting patterns. According to the broken symmetries, we find two different instabilities of the homogeneous state. One is harmonic with respect to external modulation and the second one is subharmonic, depending on the parameters. The harmonic solution is a continuous deformation of the homogeneous solution of the unforced system, whereby the new subharmonic solution occurs only in a finite range of the forcing amplitude. At special parameter values both instabilities have the same threshold and one has a so-called codimension-two bifurcation of a similar type as investigated recently [16]. Since both patterns have a different symmetry with respect to translations by one wavelength of the modulation, the harmonic one is symmetric and the subharmonic one antisymmetric, they coexist beyond threshold in a wide range of parameters. According to this coexistence there are surprising phenomena, such as stable propagating pulses of subharmonic patterns in a harmonic background or traveling phase flips connecting the two alternative subharmonic patterns.

Modified amplitude equation. – Oscillating fields $u(x, t)$ near onset may be separated into a fast oscillation $\exp[i\omega_c t]$ and the slow dynamics of the amplitude $A(x, t)$ as $u(x, t) \sim A(x, t) \exp[i\omega_c t] + \text{c.c.}$, where ω_c is the natural frequency. The dynamics of the amplitude $A(x, t)$ near a supercritical Hopf bifurcation is described by the Complex-Ginzburg-Landau Equation (CGLE). Near-resonant temporal forcing with a frequency $\omega_{\text{ext}} = 2(\omega_c - \nu)$ with a small detuning ν leads to the following model [8]:

$$\partial_t A = \left[\varepsilon + i\nu + (1 + ib)\Delta - (1 + ic) |A|^2 \right] A + \gamma_{\text{het}}(x) A^*, \quad (1)$$

where $\gamma_{\text{het}}(x)$ represents the spatially varying forcing amplitude. For an unforced system the oscillatory instability appears for $\varepsilon_c > 0$. Linear and nonlinear dispersion of the frequency are described by b and c . The modulation is chosen as a superposition of a constant offset and a spatially periodic part:

$$\gamma_{\text{het}}(x) = \gamma_0 + \gamma_1(x) = \gamma_0 + 2G \cos(2kx). \quad (2)$$

For this case eq. (1) exhibits two fundamental spatially varying solutions with different symmetries: One is symmetric with respect to translations by one wavelength $\lambda = \pi/k$ of the forcing, $A(x, t) = A(x + \pi/k, t)$ (harmonic with respect to the spatial modulation) and the other one is antisymmetric, $A(x, t) = -A(x + \pi/k, t)$ (subharmonic).

A possible experimental realization of the modulated forcing is sketched in fig. 1: a light sensitive, oscillatory chemical reaction is forced by shining light with time-periodic variations of the intensity onto the sample. A spatial modulation of the forcing is achieved by introducing a filter with spatially varying transmission properties.

Linear stability analysis. – The solution of the linear part of eq. (1) has an exponential time dependence and for small values of the modulation amplitude $G = \delta\bar{G}$, with $\delta \ll 1$ and $\bar{G} \sim O(1)$, its amplitude may be expanded with respect to δ :

$$A = e^{\sigma t} (A_0 + \delta A_1 + \delta^2 A_2 + \dots) . \quad (3)$$

The neutral stability condition, $\text{Re}(\sigma) = 0$, determines the critical value of the control parameter ε_c which separates the parameter range where the ground state, $A = 0$, is stable from the range where $A = 0$ is unstable. Both ε_c and ω_c depend on the modulation amplitude and are expanded with respect to small values of δ :

$$\varepsilon_c = \varepsilon_c^{(0)} + \delta\varepsilon_c^{(1)} + \delta^2\varepsilon_c^{(2)} + \dots , \quad (4)$$

$$\omega_c = \omega_c^{(0)} + \delta\omega_c^{(1)} + \delta^2\omega_c^{(2)} + \dots . \quad (5)$$

The expansions given in eqs. (2)-(5) together with eq. (1) provide the following hierarchy of equations defining the neutral stability ($\text{Re}(\sigma) = 0$) of the ground state:

$$\delta^0 : \mathcal{L}_0 A_0 + \gamma_0 A_0^* = -\omega_c^{(0)} A_0 , \quad (6)$$

$$\delta^1 : \mathcal{L}_0 A_1 + \gamma_0 A_1^* = -[\varepsilon_c^{(1)} + i\omega_c^{(1)}]A_0 - \gamma_1(x)A_0^* , \quad (7)$$

$$\delta^2 : \mathcal{L}_0 A_2 + \gamma_0 A_2^* = -[\varepsilon_c^{(2)} + i\omega_c^{(2)}]A_0 , \quad (8)$$

with $\mathcal{L}_0 = \varepsilon_0 + i\nu + (1 + ib)\Delta$. These equations may be solved by profiles which are either harmonic (h)

$$A_0 = F_0 , \quad A_1 = F_2 e^{2ikx} + F_{-2} e^{-2ikx} \dots \quad (9)$$

or subharmonic (sh)

$$A_0 = F_1 e^{ikx} + F_{-1} e^{-ikx} , \quad A_1 = F_3 e^{3ikx} + F_{-3} e^{-3ikx} \dots \quad (10)$$

with respect to $\gamma_{\text{het}}(x)$. Equation (6) leaves the amplitudes F_0 and $F_{1,-1}$ undetermined, but it fixes the corresponding critical values $\varepsilon_c^{(0)}$ and $\omega_c^{(0)}$. The right-hand sides of eqs. (7) and (8) contain contributions which belong to the kernel of the operator at the left-hand side. Thus, they are subject to a solvability condition which determines the next-order corrections $\varepsilon_c^{(1),(2)}$ and $\omega_c^{(1),(2)}$. For that purpose A_1 has to be calculated from eq. (7), but A_2 is not needed. In order to distinguish the harmonic and subharmonic case, we introduce ε_h, ω_h , respectively $\varepsilon_{\text{sh}}, \omega_{\text{sh}}$, which replace ε_c, ω_c in the corresponding computation. Collecting all terms up to the power G^2 , one obtains finally the modulation-induced shift of threshold and frequency for the harmonic case:

$$\varepsilon_h + i\omega_h = -\gamma_0 - i\nu - 2G^2 \frac{2(\gamma_0 + 2k^2) + i(\nu - 4bk^2)}{8\gamma_0 k^2 + 16k^4 + (\nu - 4bk^2)^2} , \quad (11)$$

and for the subharmonic case

$$\varepsilon_{\text{sh}} + i\omega_{\text{sh}} = k^2 - R - G - G^2 \frac{\gamma_0 + R + 8k^2 + i(9bk^2 - \nu)}{16k^2 [k^2 (4 + 5b^2) - \nu b + R]} , \quad (12)$$

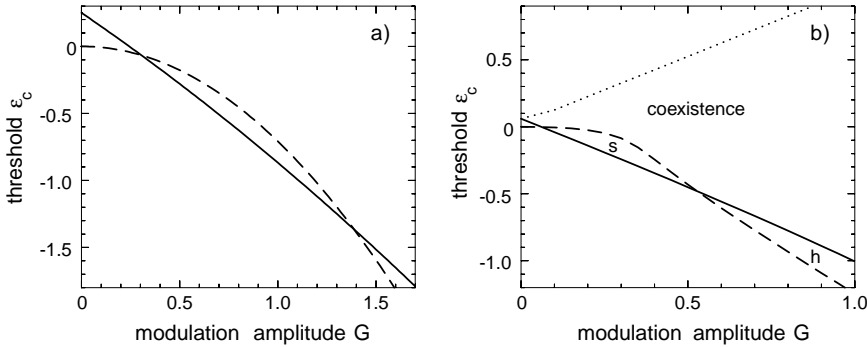


Fig. 2 – In part a) the analytical threshold for harmonic ε_h (dashed line) and subharmonic ε_{sh} (solid line) patterns are shown as a function of the modulation amplitude G according to eqs. (11), (12) and for the parameters $\nu = bk^2$, $k = 1/2$, $b = 1.8$ and γ_0 . In b) the threshold for the subharmonic (solid line) and the harmonic (dashed line) patterns are shown as obtained by the full numerical solution of the linear part of eq. (1) and for the parameters $\nu = bk^2$, $k = 4\pi/51$, $b = 8$, γ_0 and $c = 2$. Solely subharmonic solutions are found in the range s and solely harmonic solutions in the range h. The upper dotted line marks the upper end of the existence region of subharmonic patterns.

with the abbreviation $R = \sqrt{\gamma_0^2 - (\nu - bk^2)^2}$. The two thresholds ε_h and ε_{sh} according to these formulas are plotted in fig. 2a). For arbitrary modulation amplitudes the linear stability analysis of the homogeneous state is performed numerically and the results of that are shown in fig. 2b). The numerically found thresholds for the harmonic and subharmonic pattern agree at the two codimension-two points (CTP) at $G_1 \simeq 0.28$ and at $G_2 \simeq 2.55$. In comparison, $G_1 \simeq 0.31$ and $G_2 \simeq 1.39$ are obtained according to the perturbative calculation. In the range $G_1 < G < G_2$ the subharmonic solution has the lower threshold. For the special choice $\nu = bk^2$ the condition $\varepsilon_h = \varepsilon_{sh}$ with formulas given in eqs. (12) and (11) leads to a polynomial quadratic for the modulation amplitude G :

$$0 = k^2 - G - \frac{G^2}{k^2} \left[\frac{1}{8} \frac{\gamma_0 + 4k^2}{\gamma_0 + 4k^2(1 + b^2)} - \frac{4(\gamma_0 + 2k^2)}{8\gamma_0 + k^2(16 + 9b^2)} \right]. \quad (13)$$

This has two real solutions $G_{1,2}$ and there is only a finite range in G where subharmonic solutions are preferred, namely if the following inequality is fulfilled:

$$1 + \frac{1}{2} \frac{\gamma_0 + 4k^2}{\gamma_0 + 4k^2(1 + b^2)} - \frac{16(\gamma_0 + 2k^2)}{8\gamma_0 + k^2(16 + 9b^2)} > 0. \quad (14)$$

For $\gamma_0 = 0$ this inequality reduces to $|b| > \sqrt{(5 + \sqrt{1177})/36} \sim 1$, whereas the full numerics provides the condition $|b| > 2$. Regions solely supporting subharmonic patterns are hence only found if the linear dispersion b in eq. (1) is non-vanishing.

Numerical results. – Harmonic and subharmonic patterns obtained by numerical integration of eq. (1) beyond threshold are shown in fig. 3. With increasing values of the modulation amplitude G the homogeneous solution of eq. (1) becomes progressively modulated with the same wavelength as the external modulation. Simultaneously the oscillation frequency is shifted. Subharmonic patterns are dominated by the mode with twice the wavelength of the external forcing and with the choice of $\nu = bk^2$ as in fig. 3 these solutions of eq. (1) are stationary.

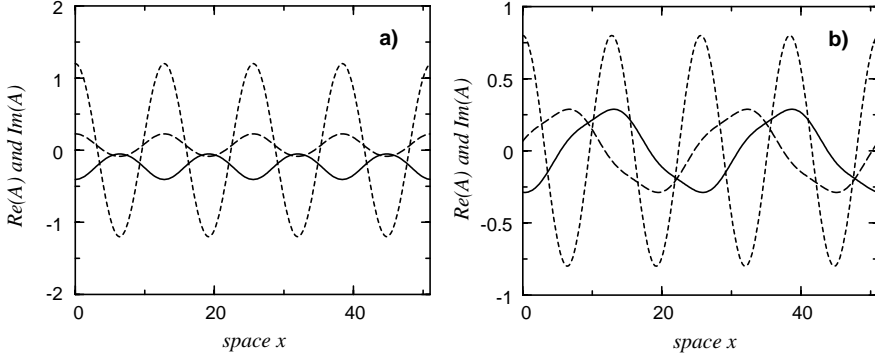


Fig. 3 – Harmonic ($G = 0.6$, panel a)) and subharmonic ($G = 0.4$, panel b)) solutions from numerical simulations at parameters $\nu = bk^2$, $k = 4\pi/51$, $b = 8$, $c = 2$, $\gamma_0 = 0$, $\varepsilon = -0.25$. the dashed lines depict the spatially dependent forcing $\gamma_{\text{het}}(x)$ and the full (long-dashed) lines show the real (imaginary) part of $A(x)$.

The term “coexistence” in fig. 2 indicates that these two solutions coexist, namely in the range above the two thresholds and below the dotted line. Coexistence means that both patterns are stable in their respective subspace, *i.e.* the harmonic pattern is stable in the subspace of modes symmetric with respect to the forcing and the subharmonic pattern is stable in the subspace of antisymmetric modes. This property may lead to more complex patterns, see, for instance, the space-time plot in fig. 4, where the harmonic and subharmonic patterns are found in neighboring regions. They are separated by two propagating domain boundaries. Such “drifting domains” have recently been studied extensively near a codimension-2 Turing-wave bifurcation in a different model [16]. The harmonic pattern at one side of the domain boundary behaves like a standing wave and the subharmonic part like a stationary structure, but the domain wall itself propagates and is stable. The temporal behavior as well as the spatial structure of two fundamental patterns can be recognized clearly from the temporal evolution of the phase plotted in fig. 4, where one can see again that the subharmonic structure

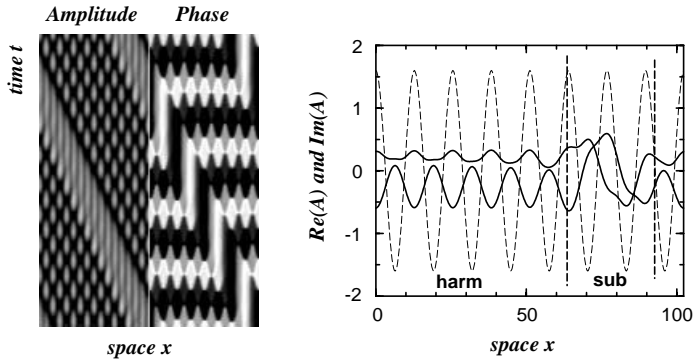


Fig. 4 – Space-time plot (left) of a subharmonic pulse in a harmonic background, with propagating fronts separating both. The right part shows at a fixed time the spatial dependence of $\text{Re}(A(x, t))$, $\text{Im}(A(x, t))$ (solid lines) and the spatial modulation $\gamma_{\text{het}}(x)$ (dashed line). Parameters are $G = 0.8$, $\varepsilon = 0.25$, $\nu = bk^2$, $L = 102.2$, $b = 8$, $c = 2$, $k = 4\pi/51$.

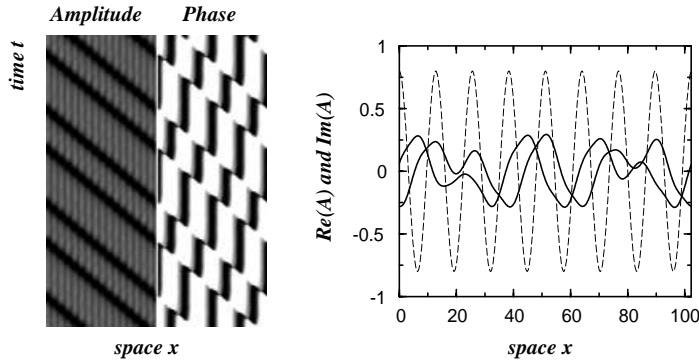


Fig. 5 – The space-time plot (left) shows traveling phase kinks in the subharmonic state. The right part shows at a certain time the spatial structure of $\text{Re}(A(x))$, $\text{Im}(A(x))$ (solid lines) and the modulation $\gamma_{\text{het}}(x)$ (dashed line). Parameters are $G = 0.4$, $\varepsilon = -0.25$, $\nu = bk^2$, $L = 102.2$, $b = 8$, $c = 2$, $k = 4\pi/51$.

is stationary, whereas the harmonic pattern behaves like a standing wave. Subharmonic patterns which differ by a phase $\phi = \pi$ are degenerate. Such equivalent patterns are also connected by a propagating domain as shown in fig. 5. The results described so far belong to the parameter range $bc > -1$, where the unforced system is Benjamin-Feir stable. The preference for a subharmonic solution at threshold depends only on the linear dispersion b and not on c (cf. eq. (14)). On the other hand, for large values of the control parameter ε the modulation $\gamma_{\text{het}}(x)$ becomes less important and again the Benjamin-Feir turbulent solution regime is expected in the range $bc < -1$. Such a transition scenario is shown in fig. 6. At threshold one has (for $b = 8$ and $c = -1$) subharmonic patterns. For the special choice

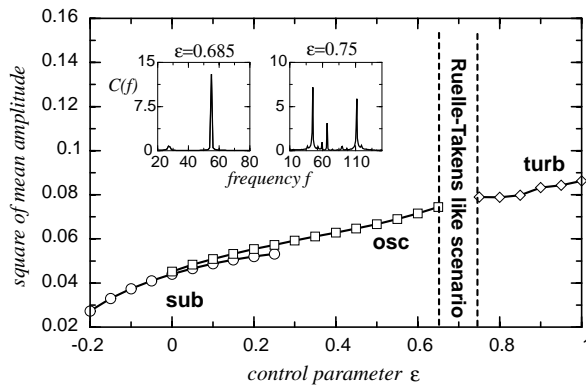


Fig. 6 – With increasing values of ε and for $bc = -8 < -1$ ($c = -1$ and $b = 8$) a transition from the subharmonic solution at threshold to a Benjamin turbulent regime far beyond threshold is shown. For $bc = -8$ and without a modulation the solutions of eq. (1) belong to the Benjamin-Feir turbulent regime. With modulation $G = 0.35$ the subharmonic solution has the lowest threshold and is the preferred solution. However, with increasing values of ε the effect of the modulation becomes less and less important and more and more temporal frequencies are excited. The power spectra of a time series of $\int |A(x, t)| dx$ for $\varepsilon = 0.685$ and $\varepsilon = 0.75$ are shown in the insets. The transition to the Benjamin-Feir turbulence has similarities to the Ruelle-Takens scenario.

$\nu = bk^2$ as in fig. 6 the subharmonic pattern is stationary and the averaged quantity $\overline{A}(t) := \int |A(x,t)| dx$ too. Beyond $\varepsilon = 0.275$ the subharmonic solution becomes unstable and $\overline{A}(t)$ starts to oscillate. For even larger values of ε , *e.g.* $\varepsilon = 0.685$, this oscillatory solution becomes unstable with respect to a second subharmonic frequency as indicated by the power spectrum shown in the first inset in fig. 6. Increasing ε further the power spectrum of $\overline{A}(t)$ develops more and more substructures as shown by the second inset in fig. 6 at $\varepsilon = 0.75$. Finally, for $\varepsilon > 0.75$ the effect of the modulation γ_{het} becomes weak and the system behaves very similarly to the unmodulated system in the Benjamin-Feir regime.

Conclusion. – It has been demonstrated that spatio-temporal forcing of oscillatory media can be employed to design patterns of a prescribed length scale. The system studied in this paper admits two different classes of patterns which are distinguished by their adjustment to the spatially modulated forcing: symmetric harmonic patterns and anti-symmetric subharmonic patterns with respect to a shift by one forcing wavelength. The instabilities of the homogeneous state giving rise to these two types of patterns have been investigated analytically and numerically. Good agreement of the two approaches is found for small forcing amplitudes. The resulting phase diagram for the existence of these patterns illustrates a competition between the oscillatory dynamics and the modulated forcing. For strong forcing, the system chooses to respond with a harmonic pattern and is dominated by the external stimulus. For weak forcing, the system has more freedom to respond —subharmonic patterns, phase slips and mixed structures are observed in an extended parameter regime. Spatio-temporal forcing can also be used to suppress spatio-temporal chaos in the CGLE near onset. A Ruelle-Takens-like scenario leading to irregular patterns is then observed far from onset.

REFERENCES

- [1] KELLY R. E. and PAL D., *J. Fluid Mech.*, **86** (1978) 433; LOWE M., GOLLUB J. P. and LUBENSKY T., *Phys. Rev. Lett.*, **51** (1983) 786; COULLET P., *Phys. Rev. Lett.*, **56** (1986) 724; ZIMMERMANN W. *et al.*, *Europhys. Lett.*, **24** (1993) 217.
- [2] ZIMMERMANN W. and SCHMITZ R., *Phys. Rev. E*, **53** (1996) R1321; ZIMMERMANN W., PAINTER B. and BEHRINGER R., *Eur. Phys. J. B*, **5** (1998) 757.
- [3] ZIMMERMANN W., SESSELBERG M. and PETRUCCIONE F., *Phys. Rev. E*, **48** (1993) 2699; HOWLE L., BEHRINGER R. P. and GEORGIADIS J. G., *Nature*, **362** (1993) 230; PAINTER B. and R. P. BEHRINGER, *Europhys. Lett.*, **44** (1998) 599.
- [4] STEINBOCK O., KETTUNEN P. and SHOWALTER K., *Science*, **269** (1995) 1857.
- [5] BÄR M. *et al.*, *J. Phys. Chem.*, **100** (1996) 19106.
- [6] SENDINA-NADAL I. *et al.*, *Phys. Rev. Lett.*, **80** (1998) 5437; *Phys. Rev. E*, **58** (1998) 1183.
- [7] RIECKE H., CRAWFORD J. D. and KNOBLOCH E., *Phys. Rev. Lett.*, **61** (1988) 1942; WALGRAEF D., *Europhys. Lett.*, **7** (1988) 485; REHBERG I. *et al.*, *Phys. Rev. Lett.*, **61** (1988) 24.
- [8] COULLET P. *et al.*, *Phys. Rev. Lett.*, **65** (1990) 1352; COULLET P. and EMILSON K., *Physica D*, **61** (1992) 119; *Physica A*, **188** (1992) 190.
- [9] ELPHICK C., HAGBERG A. and MERON E., *Phys. Rev. Lett.*, **80** (1998) 5007; *Phys. Rev. E*, **59** (1999) 5285.
- [10] CHATE H., RUDZICK O. and PIKOVSKY A., *Physica D*, **131** (1999) 17.
- [11] PETROV V., QUYANG Q. and SWINNEY H. L., *Nature*, **388** (1997) 655.
- [12] LIN A. L. *et al.*, *Phys. Rev. Lett.*, **84** (2000) 4240; *Phys. Rev. E*, **62** (2000) 3790.
- [13] KADAR S., WANG J. and SHOWALTER K., *Nature*, **391** (1998) 770.
- [14] JUNG P. and MAYER-KRESS G., *Phys. Rev. Lett.*, **74** (1995) 2140.
- [15] HEMMING C. J. and KAPRAL R., *Chaos*, **10** (2000) 720.
- [16] NICOLA E. *et al.*, preprint nlin.PS/0005043, submitted (2000).